

Static and dynamic analysis of non-circular helicoidal bars with cruciform cross-sections via mixed FEM

*Merve Ermis¹, Murat Yılmaz², Nihal Eratlı³ and Mehmet H. Omurtag⁴

1), 2), 3), 4) *Faculty of Civil Engineering, Istanbul Technical University, Istanbul, Turkey*

¹⁾ ermism@itu.edu.tr

ABSTRACT

In this study, the static and dynamic analyses of non-circular (conical, hyperboloidal, barrel) helicoidal bars having cruciform cross section are investigated via mixed finite element formulation. The torsional moment of inertia for cruciform section is calculated by finite element solution of Poisson's equation. Helicoidal rod domain is discretized with a two-noded curved element. Each node of the curved element has 12 degrees of freedom, and they are three translations, three rotations, two shear forces, one axial force, two bending moment and one torque. Timoshenko beam theory is used as field equations and exact curvatures at the nodal points are used by interpolation through the element via linear shape functions for generating the element matrix. In this study, non-circular helicoidal bars with fixed-fixed and fixed-free boundary conditions having thin and moderately thick cruciform cross-sections are handled. Through the analysis the influence of the cross-sectional geometry and the boundary conditions on the static and dynamic behavior of the non-circular helicoidal bars is investigated.

1. INTRODUCTION

In the literature, the static and the dynamic analysis of the non-cylindrical helices with the circular and the rectangular cross-sections are available. In order to address these helix problems, various numerical methods were employed such as the finite element method (Mottershead 1980, Omurtag and Aköz 1992, Girgin 2006, Eratlı et al. 2015), the transfer matrix method (Pearson 1982, Yıldırım 1996) which is the most popular ones. The transfer matrix method is applied to dynamic analysis of cylindrical/non-cylindrical helical springs besides finite element method with circular and rectangular cross-sections in Yıldırım and İnce (1997), Yıldırım (1997), Yıldırım (1998) and Yıldırım (2002). Busool and Eisenberger (2002) analyzed the free vibration of non-cylindrical helicoidal bars with circular and rectangular variable cross-sections by using

¹ Research Assistant

² PhD

³ Associate Professor

⁴ Professor

the exact element method. Using the pseudospectral method Lee (2007) investigated the free vibration of non-cylindrical helical springs with circular cross-sections.

Geometry of the helicoidal bars lets them to be forced under considerable torque. Thus precise torsional rigidity of calculation of non-circular cross sections are very important in obtaining the results with necessary high precision. The exact value of torsional rigidity limited to a few cross sections like rectangular, ellipse and equilateral triangle (Timoshenko and Goodier 1969). To obtain analytical solutions for the arbitrary cross-sections are cumbersome. Therefore some numerical studies are performed to overcome this problem. The torsional rigidity problem was solved by the finite difference, finite element and boundary element methods (Ely and Zienkiewicz 1960, Wang 1953, Hermann 1965, Krahula and Lauterbach 1969, Darilmaz et al. 2007, Li et al. 2000, Eratlı et al. 2016, Sapountzakis 2001, Sapountzakis and Mocos 2004).

In this study, static and dynamic analysis of conical, barrel and hyperboloidal helices having cruciform cross-section are performed via the mixed finite element algorithm verified by Eratlı et al. (2016). This algorithm is based on the Timoshenko beam theory. The torsional rigidity of the cruciform cross-section is calculated by finite element solution of Poisson's equation. The displacement, rotation shear force, moment and the first six natural frequencies of non-circular helices are presented as an benchmark examples for the literature.

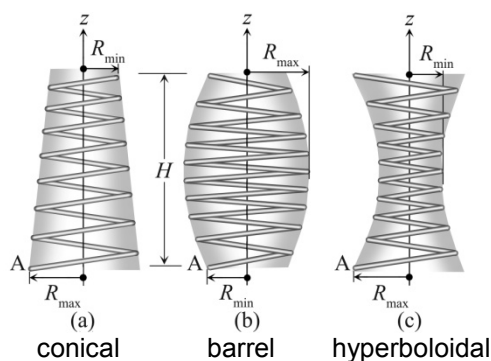


Fig. 1 Non-circular helix geometries

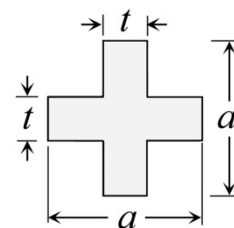


Fig. 2 Cruciform cross-section

2. FORMULATION

2.1 Helix Geometry

The geometrical properties of the helices in Figure 1 are $x = R(\varphi)\cos\varphi$, $y = R(\varphi)\sin\varphi$, $z = p(\varphi)\varphi$, $p(\varphi) = R(\varphi)\tan\alpha$, where α denotes the pitch angle, $R(\varphi)$ and $p(\varphi)$ signify the centerline radius and the step for unit angle, respectively, of the helix as a function of the horizontal angle φ . With $c(\varphi) = \sqrt{R^2(\varphi) + p^2(\varphi)}$, the infinitesimal arc length becomes $ds = c(\varphi)d\varphi$. The Frenet unit vectors are as follows: \mathbf{t} is the tangent unit vector, \mathbf{n} is the normal unit vector, $\mathbf{b} = \mathbf{t} \times \mathbf{n}$ is the binormal unit vector. In the case of a conical helix, the radius at any point on the helix geometry is $R(\varphi) = R_{\max} + (R_{\min} - R_{\max})(\varphi/2n\pi)$ where n is the number of active turns, R_{\max} and R_{\min} are the bottom radius and top radius, respectively, of the conical helix geometry and in

the case of a barrel, the radius is $R(\varphi) = R_{\max} + (R_{\min} - R_{\max}) (1 - \varphi/n\pi)^2$, R_{\min} and R_{\max} are the bottom radius and the central radius, respectively or in the case of hyperboloidal helix, the radius is $R(\varphi) = R_{\min} + (R_{\max} - R_{\min}) (1 - \varphi/n\pi)^2$, where R_{\max} and R_{\min} are the bottom radius and the central radius, respectively.

2.2 The field equations and the functional

The field equations based on Timoshenko beam theory for the elastic helix in the Frenet coordinate system exist in Eratlı et al. (2016).

$$\left. \begin{aligned} -\mathbf{T}_{,s} - \mathbf{q} + \rho A \ddot{\mathbf{u}} &= \mathbf{0} \\ -\mathbf{M}_{,s} - \mathbf{t} \times \mathbf{T} - \mathbf{m} + \rho \mathbf{I} \ddot{\mathbf{\Omega}} &= \mathbf{0} \end{aligned} \right\} \quad (1)$$

$$\left. \begin{aligned} \mathbf{u}_{,s} + \mathbf{t} \times \mathbf{\Omega} - \mathbf{C}_{\gamma} \mathbf{T} &= \mathbf{0} \\ \mathbf{\Omega}_{,s} - \mathbf{C}_{\kappa} \mathbf{M} &= \mathbf{0} \end{aligned} \right\} \quad (2)$$

where $\mathbf{u} = u_t \mathbf{t} + u_n \mathbf{n} + u_b \mathbf{b}$ is the displacement vector, $\mathbf{\Omega} = \Omega_t \mathbf{t} + \Omega_n \mathbf{n} + \Omega_b \mathbf{b}$ is the rotational vector, $\ddot{\mathbf{u}} = \partial^2 \mathbf{u} / \partial t^2$ and $\ddot{\mathbf{\Omega}} = \partial^2 \mathbf{\Omega} / \partial t^2$ are the accelerations of the translations and rotations of the equation of motion, respectively. $\mathbf{T} = T_t \mathbf{t} + T_n \mathbf{n} + T_b \mathbf{b}$ is the force vector, $\mathbf{M} = M_t \mathbf{t} + M_n \mathbf{n} + M_b \mathbf{b}$ is the moment vector, ρ is the density of material, A is the area of the cross-section, \mathbf{I} is the moment of inertia tensor, \mathbf{C} is the compliance matrix, \mathbf{q} and \mathbf{m} are the distributed external force vector and moment vector, respectively. Eqs. (1)-(2) can be written in operator form as $\mathbf{Q} = \mathbf{L}\mathbf{y} - \mathbf{f}$. After proving the operator to be potential, the functional yields to the following form

$$\left. \begin{aligned} \mathbf{I}(\mathbf{y}) = & - \left[\mathbf{u}, \frac{d\mathbf{T}}{ds} \right] + \left[\mathbf{t} \times \mathbf{\Omega}, \mathbf{T} \right] - \left[\frac{d\mathbf{M}}{ds}, \mathbf{\Omega} \right] - \frac{1}{2} \left[\mathbf{C}_{\kappa} \mathbf{M}, \mathbf{M} \right] - \frac{1}{2} \left[\mathbf{C}_{\gamma} \mathbf{T}, \mathbf{T} \right] \\ & - \frac{1}{2} \rho A \omega^2 \left[\mathbf{u}, \mathbf{u} \right] - \frac{1}{2} \rho \omega^2 \left[\mathbf{I} \mathbf{\Omega}, \mathbf{\Omega} \right] - \left[\mathbf{q}, \mathbf{u} \right] - \left[\mathbf{m}, \mathbf{\Omega} \right] \\ & + \left[\left(\mathbf{T} - \hat{\mathbf{T}} \right), \mathbf{u} \right]_{\sigma} + \left[\left(\mathbf{M} - \hat{\mathbf{M}} \right), \mathbf{\Omega} \right]_{\sigma} + \left[\hat{\mathbf{u}}, \mathbf{T} \right]_{\varepsilon} + \left[\hat{\mathbf{\Omega}}, \mathbf{M} \right]_{\varepsilon} \end{aligned} \right\} \quad (3)$$

where ω is the natural circular frequency and the square parentheses indicate the inner product. The terms with hats in Eq. (3) are known values on the boundary and the subscripts ε and σ represent the geometric and the dynamic boundary conditions, respectively. Considering the harmonic motion of the helix in the free vibration analysis, \mathbf{q} and \mathbf{m} are equal zero.

2.3 Finite Element Formulation of the Torsion Problem

By introducing scalar field function Φ , the governing equation for the torsion problem (Poisson's equation) is

$$\Phi_{,11} + \Phi_{,22} = -2 \quad (4)$$

with $\Phi = 0$ on Γ the boundary. Defining a vector field Ξ on Ω^e as $\Xi = \{\psi_i \Phi_{,1}^e, \psi_i \Phi_{,2}^e\}^T$ and using the divergence theorem the weak form of the Eq. (4) can be constructed as,

$$\int_{\Omega^e} (\psi_{i,1} \Phi_{,1}^e + \psi_{i,2} \Phi_{,2}^e) d\Omega^e = 2 \int_{\Omega^e} \psi_i d\Omega^e + \oint_{\Gamma^e} \psi_i \nabla \Phi^e \cdot \mathbf{n}^e d\Gamma^e \quad (5)$$

The boundary terms in Eq. (5) cancel out during the assemblage of the finite element equations for adjacent element edges in the cross-section domain Ω and they are also zero on the free edges (edges without an adjacent element) to satisfy the boundary condition of the torsion problem. The torsional constant I_t of the cross-section, in terms of the scalar field, is expressed as,

$$I_t = - \int_{\Omega} (\Phi_{,1} x_1 + \Phi_{,2} x_2) d\Omega \quad (6)$$

which renders to the summation given with the following equation over domain elements as,

$$\mu I_3 = - \sum_{e=1}^N \mu^e \int_{\Omega_\eta^e} \Phi^T [\partial \Psi] [\mathbf{J}]^{-1} [\mathbf{X}] \Psi |\det[\mathbf{J}]| d\Omega_\eta^e \quad (7)$$

where $[\partial \Psi]$ with the definition,

$$[\partial \Psi] = \begin{bmatrix} \partial \psi_1 / \partial \eta_1 & \partial \psi_1 / \partial \eta_2 \\ \partial \psi_2 / \partial \eta_1 & \partial \psi_2 / \partial \eta_2 \\ \vdots & \vdots \\ \partial \psi_9 / \partial \eta_1 & \partial \psi_9 / \partial \eta_2 \end{bmatrix} \quad (8)$$

where $[\mathbf{J}]$ (Jacobian matrix) is calculated with $[\mathbf{J}] = [\mathbf{X}] [\partial \Psi]$, $[\mathbf{X}]$ being the nodal coordinates matrix, and Φ is the vector with the scalar field nodal-values as its components. Integrations are performed with the $3 \times 3 = 9$ point Gauss quadrature rule. $\mu = G$ is the shear modulus and N is the total number of elements.

2.4 Mixed Finite Element Formulation

Linear shape functions are $\phi_i = (\varphi_j - \varphi) / \Delta \varphi$ and $\phi_j = (\varphi - \varphi_i) / \Delta \varphi$ are used in finite element formulation. The subscripts represent node numbers of the bar element and $\Delta \varphi = (\varphi_j - \varphi_i)$. The curvatures are satisfied exactly at the nodal points and linearly interpolated through the element. The curved bar element has two nodes with 2×12 degrees of freedom. The variable vector per node is as follows:

$$\mathbf{X}^T = \{u_t, u_n, u_b, \Omega_t, \Omega_n, \Omega_b, T_t, T_n, T_b, M_t, M_n, M_b\} \quad (9)$$

The problem of determining the natural frequencies of a structural system reduces to the solution of a standard eigenvalue problem $([\mathbf{K}] - \omega^2 [\mathbf{M}]) \{\mathbf{u}\} = \{\mathbf{0}\}$ where $[\mathbf{K}]$ is the system matrix, $[\mathbf{M}]$ is the mass matrix for the entire domain, \mathbf{u} is the eigenvector (mode shape) and ω is the natural angular frequency of the system. Hence the explicit form of standard eigenvalue problem in the mixed formulation is

$$\begin{pmatrix} [\mathbf{K}_{11}] & [\mathbf{K}_{12}] \\ [\mathbf{K}_{22}] & [\mathbf{K}_{22}] \end{pmatrix} - \omega^2 \begin{pmatrix} [\mathbf{0}] & [\mathbf{0}] \\ [\mathbf{0}] & [\mathbf{M}] \end{pmatrix} \begin{Bmatrix} \{\mathbf{F}\} \\ \{\mathbf{U}\} \end{Bmatrix} = \begin{Bmatrix} \{\mathbf{0}\} \\ \{\mathbf{0}\} \end{Bmatrix} \quad (10)$$

where $\{\mathbf{F}\}$ denotes the nodal force and the moment vectors and $\{\mathbf{U}\} = \{\mathbf{u} \ \boldsymbol{\Omega}\}^T$ signifies the nodal displacement and rotation vectors. To attain consistency between Eq. (10) and $([\mathbf{K}] - \omega^2[\mathbf{M}])\{\mathbf{u}\} = \{\mathbf{0}\}$, the $\{\mathbf{F}\}$ vector is eliminated in Eq. (10), which yields to the condensed system matrix $[\mathbf{K}^*] = [\mathbf{K}_{22}] - [\mathbf{K}_{12}]^T[\mathbf{K}_{11}]^{-1}[\mathbf{K}_{12}]$. Finally, the eigenvalue problem in the mixed formulation becomes $([\mathbf{K}^*] - \omega^2[\mathbf{M}])\{\mathbf{U}\} = \{\mathbf{0}\}$.

3. NUMERICAL EXAMPLES

The fixed-fixed and fixed-free boundary conditions are used. The material and geometric properties of the helices are: the modulus of elasticity $E = 210 \text{ GPa}$, Poisson's ratio $\nu = 0.3$, the density of material $\rho = 7850 \text{ kg/m}^3$, the number of active turns $n = 6.5$, the pitch angle $\alpha = 4.8^\circ$, the ratio of the minor radius to the major radius of the helix $R_{\min} / R_{\max} = 0.5$ (where $R_{\min} = 13 \text{ mm}$). The cruciform cross-section (see Fig. 2) with two different thickness-to-side ratios $t/a = 1/5$ and $t/a = 1/3$ where $a = 2 \text{ mm}$ is considered. Referring to these two different t/a ratios, the computed torsional inertia moments are $I_t = 0.00519a^4$ and $I_t = 0.02313a^4$, respectively (Eratlı et al. 2016). In the static analysis, the helices are analyzed by considering that it is subjected to a uniformly distributed loading. The intensity of the uniform load is taken as $q_z = 0.01 \text{ N/m}$. As a result of a convergence analysis it is observed that 200 elements yield to necessary precision.

3.1 Dynamic Analysis

The scope of this example is to investigate the effects of the thickness-to-side ratios of the cruciform cross-section and the boundary conditions on the dynamic behavior of the non-circular helicoidal bars (barrel and conical helices). The material and geometrical properties of these helices are identical to the hyperboloidal helix solved in Eratlı et al. (2016). For the fixed-fixed and the fixed free boundary conditions, the first six natural frequency results of the barrel and conical helices having the cruciform cross-section are tabulated in Tables 1-2 where the first six natural frequencies are also verified with SAP2000. In the case of the fixed-fixed boundary condition, the increase of the fundamental natural frequency of the $t/a=1/3$ cross-section with respect to for the $t/a=1/5$ cross-section is 70% and 69% for both the barrel and the conical type helices, respectively. In the case of the fixed-free boundary condition, with respect to the fundamental natural frequency for the $t/a=1/5$ ratio, the results of $t/a=1/3$ ratio increased by 55% and 56% for the barrel and the conical type helices, respectively. When the influence of the boundary conditions is considered the fundamental natural frequencies of the fixed-free boundary condition decreased in the range of 62%~66% with respect to the fixed-fixed boundary condition (see Tables 1-2). When the fundamental natural frequencies of the barrel type helix are compared with the fundamental natural

frequencies of the conical type helix, it is observed that, the percent increase is approximately 15% and 19% for both the fixed-fixed and the fixed-free boundary conditions, respectively.

Table 1 The natural frequencies (Hz) of barrel type helix with the fixed-fixed and fixed-free boundary conditions

		<i>t / a</i>					
		1/5			1/3		
		This study	SAP2000	diff.%	This study	SAP2000	diff.%
fixed-fixed	1	20.9	21.0	-0.48	35.5	35.7	-0.56
	2	37.9	38.0	-0.26	53.8	53.9	-0.19
	3	39.2	39.2	0.00	56.6	56.8	-0.35
	4	39.8	40.0	-0.50	57.1	57.1	0.00
	5	50.7	50.9	-0.39	66.0	66.3	-0.45
	6	54.0	54.8	-1.48	90.0	92.1	-2.33
fixed-free	1	7.7	7.7	0.00	11.9	12.0	-0.84
	2	7.9	7.9	0.00	12.1	12.1	0.00
	3	9.5	9.5	0.00	16.1	16.2	-0.62
	4	27.1	-	-	29.5	29.6	-0.34
	5	27.5	27.6	-0.36	45.9	-	-
	6	28.8	28.9	-0.35	48.2	48.5	-0.62

diff.% = (This study-SAP2000)×100/This study)

Table 2 The natural frequencies (Hz) of conical type helix with the fixed-fixed and fixed-free boundary conditions

		<i>t / a</i>					
		1/5			1/3		
		This study	SAP2000	diff.%	This study	SAP2000	diff.%
fixed-fixed	1	24.6	24.6	0.00	41.6	41.7	-0.24
	2	43.7	43.7	0.00	66.2	66.2	0.00
	3	47.8	47.9	-0.21	67.2	67.3	-0.15
	4	51.3	51.3	0.00	73.4	73.4	0.00
	5	65.7	65.7	0.00	81.2	81.3	-0.12
	6	67.5	67.6	-0.15	108.2	108.4	-0.18
fixed-free	1	9.4	9.4	0.00	14.7	14.7	0.00
	2	9.8	9.9	-1.02	15.1	15.2	-0.66
	3	10.9	10.9	0.00	18.2	18.2	0.00
	4	30.0	-	-	41.2	41.2	0.00
	5	34.4	34.4	0.00	50.6	-	-
	6	38.5	38.5	0.00	57.6	57.7	-0.17

diff.% = (This study-SAP2000)×100/This study)

3.2 Static Analysis

In the static analysis, the effects of the helix geometry, thickness-to-side ratios of the cruciform cross-section and the boundary conditions on the nodal variables are investigated. The maximum displacement (u_z) and the maximum rotation (Ω_z), and, fixed end reactions (T_z : shear force, M_y : moment) are used for the numerical comparisons. Finite element calculations are performed in Frenet coordinates and the results are transformed back to the global coordinates and they are verified with SAP2000 also. For the fixed-fixed and fixed-free boundary conditions, the results of the barrel, conical and hyperboloidal type helices are presented in Tables 3-5, respectively. When the maximum displacements of the conical and hyperboloidal helices are compared with the respective results of the barrel type helix, a reduction is observed. Comparison of the maximum displacements of the conical and hyperboloidal helices for the fixed-fixed boundary condition in Tables 4-5 with Table 3 for each t/a ratios reveal that the percent reductions in Tables 4-5 are approximately 29% and 41%, respectively. For the fixed-free boundary conditions, these percent reductions in Tables 4-5 are approximately 18% and 56%, respectively. The reduction of the maximum displacements of the $t/a=1/3$ cross-section with respect to for the $t/a=1/5$ cross-section is approximately 78% for all helix types and boundary conditions. When the maximum displacements of the fixed-fixed boundary condition are compared with respect to the results of the fixed-free boundary condition, the reductions are approximately 79%, 81% and 71% for the barrel, the conical and the hyperboloidal type helices, respectively.

Table 3 The displacements, rotations, forces and moments of barrel type helix with the fixed-fixed and fixed-free boundary conditions (see Fig. 1)

			max. displacements ($\times 10^{-2}$ mm)	max. rotations ($\times 10^{-4}$ rad)	shear force at point A ($\times 10^{-2}$ N)	moment at point A ($\times 10^{-4}$ Nm)
			u_z	Ω_z	T_z	M_y
fixed-fixed	1/5	This study	-6.538	-2.250	0.4440	0.590
		SAP2000	-6.475	-2.240	0.4443	0.580
		diff.%	0.96	0.44	-0.07	1.69
	1/3	This study	-1.463	-0.408	0.4440	0.590
		SAP2000	-1.447	-0.400	0.4443	0.580
		diff.%	1.09	1.96	-0.07	1.69
fixed-free	1/5	This study	-30.31	-9.706	0.8880	1.160
		SAP2000	-30.03	-9.650	0.8886	1.160
		diff.%	0.92	0.58	-0.07	0.00
	1/3	This study	-6.813	-1.731	0.8880	1.160
		SAP2000	-6.740	-1.720	0.8886	1.160
		diff.%	1.07	0.64	-0.07	0.00

diff.% = (This study-SAP2000) \times 100/This study)

Table 4 The displacements, rotations, forces and moments of conical type helix with the fixed-fixed and fixed-free boundary conditions (see Fig. 1)

			max. displacements ($\times 10^{-2}$ mm)	max. rotations ($\times 10^{-4}$ rad)	shear force at point A ($\times 10^{-2}$ N)	moment at point A ($\times 10^{-4}$ Nm)
			u_z	Ω_z	T_z	M_y
fixed-fixed	1/5	This study	-4.644	-1.666	0.3223	0.800
		SAP2000	-4.630	-1.660	0.3224	0.810
		diff.%	0.30	0.36	-0.03	-1.25
	1/3	This study	-1.038	-0.309	0.3223	0.800
		SAP2000	-1.034	-0.310	0.3229	0.810
		diff.%	0.39	-0.32	-0.19	-1.25
fixed-free	1/5	This study	-24.89	-7.813	0.7992	2.070
		SAP2000	-24.82	-7.800	0.7993	2.080
		diff.%	0.28	0.17	-0.01	-0.48
	1/3	This study	-5.590	-1.393	0.7992	2.070
		SAP2000	-5.568	-1.390	0.7993	2.080
		diff.%	-0.39	0.22	-0.01	-0.48

diff.% = (This study-SAP2000) \times 100/This study)

Table 5 The displacements, rotations, forces and moments of hyperboloidal type helix with the fixed-fixed and fixed-free boundary conditions (see Fig. 1)

			max. displacements ($\times 10^{-2}$ mm)	max. rotations ($\times 10^{-4}$ rad)	shear force at point A ($\times 10^{-2}$ N)	moment at point A ($\times 10^{-4}$ Nm)
			u_z	Ω_z	T_z	M_y
fixed-fixed	1/5	This study	-3.829	-1.362	0.3552	0.890
		SAP2000	-3.840	-1.360	0.3555	0.900
		diff.%	-0.29	0.15	-0.08	-1.12
	1/3	This study	-0.863	-0.258	0.3552	0.890
		SAP2000	-0.864	-0.260	0.3555	0.900
		diff.%	-0.12	-0.78	-0.08	-1.12
fixed-free	1/5	This study	-13.30	-4.990	0.7104	1.840
		SAP2000	-13.19	-5.000	0.7109	1.850
		diff.%	0.83	-0.20	-0.07	-0.54
	1/3	This study	-3.004	-0.890	0.7104	1.840
		SAP2000	-2.972	-0.890	0.7109	1.850
		diff.%	1.07	0.00	-0.07	-0.54

diff.% = (This study-SAP2000) \times 100/This study)

4. CONCLUSIONS

Static and dynamic analysis of barrel, conical and hyperboloidal helices having the cruciform cross-section is performed via the mixed finite element method. The finite

element solutions are compared using the commercial program SAP2000 and its Section Designer module. The absolute percent differences between these finite element models is in range of 0-2.33% in the case of 1000 elements by SAP2000 and 200 elements by the present mixed model. This difference is due to the used torsional rigidity of the cruciform cross-section, besides the straight SAP2000 elements and the curved elements of the present study. The compressed mesh is used to calculate the torsional inertia moment of the cruciform cross-section in the SAP2000 for $t/a=1/5$ and $t/a=1/3$ ratios and the calculated torsional inertia moments are compared with respect to our torsional inertia moments obtained in Eratlı et al. (2016). The absolute differences for the torsional inertia moments between SAP2000 and Eratlı et al. (2016) is approximately 0.20% and 0.37% for $t/a=1/5$ and $t/a=1/3$ ratios, respectively. Torsional rigidity of calculation of non-circular cross sections is very important in obtaining the results with a necessary high precision for the 3D problems. Thus, the thickness-to-side ratios of the cruciform cross-section and the boundary conditions on the static and the dynamic response of the non-circular helicoidal bars are discussed extensively.

REFERENCES

- Busool W. and Eisenberger M. (2002), "Free vibration of helicoidal beams of arbitrary shape and variable cross section", *J. Vib. Acoust.*, **124**, 397-409.
- Darılmaz, K., Orakdogan, E., Girgin, K. and Küçükarslan, S. (2007), "Torsional rigidity of arbitrarily shaped composite sections by hybrid finite element approach", *Steel Compos. Struct.*, **7**(3), 241-251.
- Ely, J.F. and Zienkiewicz, O.C. (1960), "Torsion of compound bars-A relaxation solution", *Int. J. Mech. Sci.*, **1**, 356-365.
- Eratlı, N., Ermis, M. and Omurtag, M.H., (2015), "Free vibration analysis of helicoidal bars with thin-walled circular tube cross-section via mixed finite element method", *Sigma Journal of Engineering and Natural Sciences*, **33**(2), 200-218.
- Eratlı, N., Yılmaz, M., Darılmaz, K. and Omurtag, M.H. (2016), "Dynamic analysis of helicoidal bars with non-circular cross-sections via mixed FEM", *Struct. Eng. Mech.*, **57**(2), 221-238.
- Hermann, L.R. (1965), "Elastic torsional analysis of irregular shapes", *J. Eng. Mech.-ASCE*, **91**(6), 11-19.
- Girgin K. (2006), "Free vibration analysis of non-cylindrical helices with, variable cross-section by using mixed FEM", *J. Sound Vib.*, **297**, 931-945.
- Krahula, J.L. and Lauterbach, G.F. (1969), "A finite element solution for Saint-Venant torsion", *AIAA Journal*, **7**(12), 2200-2203.
- Lee J. (2007), "Free vibration analysis of non-cylindrical helical springs by the pseudospectral method", *J. Sound Vib.*, **305**, 543-551.
- Li, Z., Ko, J.M. and Ni, Y.Q. (2000), "Torsional rigidity of reinforced concrete bars with arbitrary sectional shape", *Finite Elem. Anal. Des.*, **35**, 349-361.
- Mottershead J.E. (1980), "Finite elements for dynamical analysis of helical rods", *Int. J. Mech. Sci.*, **2**(1), 267-283.
- Omurtag M.H. and Aköz A.Y. (1992), "The mixed finite element solution of helical beams with variable cross-section under arbitrary loading", *Comput. Struct.*, **43**(2), 325-331.

- Pearson D. (1982), "The transfer matrix method for the vibration of compressed helical springs", *J. Mech. Eng. Sci.*, **24**(4), 163-171.
- Sapountzakis, E.J. (2001), "Nonuniform torsion of multi-material composite bars by the boundary element method", *Comput. Struct.*, **79**, 2805-2816.
- Sapountzakis, E.J. and Mokos, V.G. (2004), "Nonuniform torsion of bars variable cross section", *Comput. Struct.*, **82**, 703-715.
- Timoshenko, S. and Goodier, J.N. (1969), *Theory of Elasticity*, McGraw-Hill, New York.
- Wang, C.T. (1953), *Applied Elasticity*, McGraw-Hill, New York.
- Yıldırım V. (1996), "Investigation of parameters affecting free vibration frequency of helical springs", *Int. J. Numer. Meth. Eng.*, **39**(1), 99-114.
- Yıldırım V. and İnce N. (1997), "Natural frequencies of helical springs of arbitrary shape", *J. Sound Vib.*, **204**(2), 311-329.
- Yıldırım V. (1997), "Free vibration analysis of non-cylindrical coil springs by combined use of the transfer matrix and complementary functions methods", *Commun. Numer. Meth. Engng.*, **13**, 487-494.
- Yıldırım V. (1998), "A parametric study on the free vibration of non-cylindrical helical springs", *J. Appl. Mech. - T ASME*, **65**, 157-163.
- Yıldırım V. (2002), "Expressions for predicting fundamental natural frequencies of non-cylindrical helical springs", *J. Sound Vib.*, **252**(3), 479-491.